High-*Q*, submicron-confined chalcogenide microring resonators

ZHEN YANG,[1,2] RIZHEN ZHANG,[1,2] ZHIYUAN WANG,[1,2] PEIPENG XU,[1,2,7] WEI ZHANG,[1,2,8] ZHE KANG,[3,4] JIAJIU ZHENG,[5] SHIXUN DAI,[1,2] RONGPING WANG,[1,2,9] AND ARKA MAJUMDAR[5,6]

[1]*Faculty of Electrical Engineering and Computer Science, Ningbo University, Ningbo 315211, China*
[2]*Key Laboratory of Photoelectric Detection Materials and Devices of Zhejiang Province, Ningbo 315211, China*
[3]*Ningbo Research Institute, Zhejiang University, Ningbo 315100, China*
[4]*Centre for Optical and Electromagnetic Research, National Engineering Research Center for Optical Instruments, Zhejiang University, Hangzhou 310058, China*
[5]*Department of Electrical and Computer Engineering, University of Washington, Seattle, WA 98195, USA*
[6]*Department of Physics, University of Washington, Seattle, WA 98195, USA*
[7]*xupeipeng@nbu.edu.cn*
[8]*zhangwei3@nbu.edu.cn*
[9]*wangrongping@nbu.edu.cn*

Abstract: We demonstrate high quality (*Q*) factor microring resonators in high index-contrast GeSbSe chalcogenide glass waveguides using electron-beam lithography followed by plasma dry etching. A microring resonator with a radius of 90 μm shows an intrinsic *Q* factor of 4.1×10^5 in the telecom band. Thanks to the submicron waveguide dimension, the effective nonlinear coefficient was determined to be up to $\sim 110 \, \mathrm{W^{-1} m^{-1}}$ at 1550 nm, yielding a larger figure-of-merit compared with previously reported submicron chalcogenide waveguides. Such a high *Q* factor, combined with the large nonlinear coefficient and high confinement, shows the great potential of the GeSbSe microring resonator as a competitive platform in integrated nonlinear photonics.

1. Introduction

An abundance of nonlinear optical effects have been realized in integrated photonic platforms [1], revealing their potentials in many applications, including coherent telecommunication [2], quantum optics [3], spectroscopy [4], and optical frequency combs [5,6]. In recent years, tremendous efforts have been made to develop integrated nonlinear platforms using different materials, including Group IV semiconductors like silicon [7], Group III-V semiconductors like AlGaAs [8,9], and dielectrics like silicon nitride [10,11]. Many efforts have been made to develop nonlinear photonic devices on the silicon platform due to their compatibility with well-developed CMOS technology and the high-index contrast [12]. However, the silicon platform suffers from strong two-photon absorption (TPA) and TPA-induced free carrier absorption (FCA). This especially becomes serious when the material is exposed to light with a wavelength below 2.2 μm with photon energy approaching half of the optical bandgap of silicon (~1.1 eV), where the performance of the materials would be seriously deteriorated due to TPA [13]. This in turn precludes silicon from many nonlinear applications in the telecom windows. Instead, a large bandgap nonlinear material with negligible or low TPA effect, multi-efficient nonlinear processes, and low propagation loss is highly desirable.

Chalcogenide glass (ChG) with inherent wide bandgap is considered promising for nonlinear integrated optics due to their exceptionally high nonlinearities (Kerr, Raman, and Brillouin coefficients), which are two or three orders of magnitude greater than silica and comparable or

superior to silicon, low two-photon absorptions (TPA) and no free-carrier effects [14]. More importantly, ChGs have broad transparency from the visible to the mid-infrared up to 20 μm depending on the chemical compositions of the materials [15]. The bandgap value can be adjusted between 1.5 eV and 2.5 eV by changing the composition ratio of chalcogenide glass [16–18]. The inherent high refractive index (n = 2~3) enables a small mode volume without excessive radiative loss. Besides, ChGs are highly scalable and can be easily deposited on any substrates without any "lattice mismatch" issue using low-cost, large-area deposition techniques such as thermal evaporation [19]. ChGs have already been extensively used for many applications, including chemical and biological sensors [20,21], broadband supercontinuum generation [22,23], stimulated Brillouin scattering (SBS) [24–26], and Raman amplification [27]. However, so far low propagation losses of 0.05 ~ 0.5 dB/cm have been achieved only in large dimension ChG waveguides (usually widths of several micrometers) [28,29], limiting the achievable nonlinear coefficient. High index-contrast ChG waveguide with submicron mode confinement and compelling loss performance could provide large nonlinear coefficient and thus could be a very promising platform for nonlinear integrated photonics.

In this paper, utilizing a high index and nontoxic $Ge_{28}Sb_{12}Se_{60}$ platform, we demonstrate high index-contrast microring resonators on an insulator platform using electron-beam lithography followed by plasma dry etching. The resonators exhibit quality factors beyond 4.1×10^5, corresponding to a ~1.3 dB/cm propagation loss. The waveguides with submicron confinement enable a high nonlinear coefficient of $110\,W^{-1}m^{-1}$ at 1550 nm and efficient dispersion engineering for GeSbSe waveguides. The thermo-optic effect of the fabricated microring resonators is also characterized to estimate the thermal drift of the devices.

2. Design and fabrication

Figure 1(a) shows the 3D cross-sectional view of the proposed waveguide. The waveguide core is GeSbSe, cladded with air from top and side and with silicon dioxide from the bottom. The refractive index of the GeSbSe film was determined to be ~2.8 at a wavelength of 1550 nm using ellipsometry (J.A. Woollam RC2 XI+). High index-contrast and strip waveguide structure was chosen to provide both strong light confinement and efficient dispersion engineering. In this platform, the waveguide width *w* and height *h* are two parameters that can be tailored according to specific applications. Figure 1(b) presents the effective index of TE modes in the GeSbSe waveguides as a function of the width at several different waveguides heigh at a wavelength of 1550 nm. We see that an effective index above ~1.7 can be achieved over a wide range of parameter space. The dashed line represents the critical structural parameters below which the waveguide can only support the fundamental mode in transverse electric (TE) polarization. We choose the cross-sectional dimension in the submicron scale with a thickness of ChG layer *h* = 300 nm, enabling strong optical confinement of the waveguide mode in the vertical direction. Another essential factor that needs to be considered for the design is the bending loss. To extract the bending loss, we calculate the fundamental TE modes of the resonator using the finite difference method (MODE Solutions, Lumerical Inc.) as shown in Fig. 1(c). The inset of Fig. 1(c) shows the fundamental TE mode profile of a bending waveguide with a radius of 5 μm, where the waveguide width and height are 720 nm and 300 nm, respectively. Thanks to the high index-contrast of the material, the calculated radiation loss derived from the leakage of the sharp bend is negligible for a ring resonator with a radius larger than 50 μm. Such small radius will benefit more compact devices.

Figure 2(a) shows the map of group velocity dispersion (GVD), defined by $D=-(\lambda/c)\cdot(d^2n_{\mathrm{eff}}/d^2\lambda)$, as a function of the waveguide width and wavelength for a 300 nm high waveguide and TE_0 mode. The black solid curve shows the trace of the zero-dispersion wavelengths, with regions to the right side of this curve belonging to the anomalous dispersion regime. We find apparent dispersion tailoring engineering of the proposed waveguides thanks to the high index-contrast
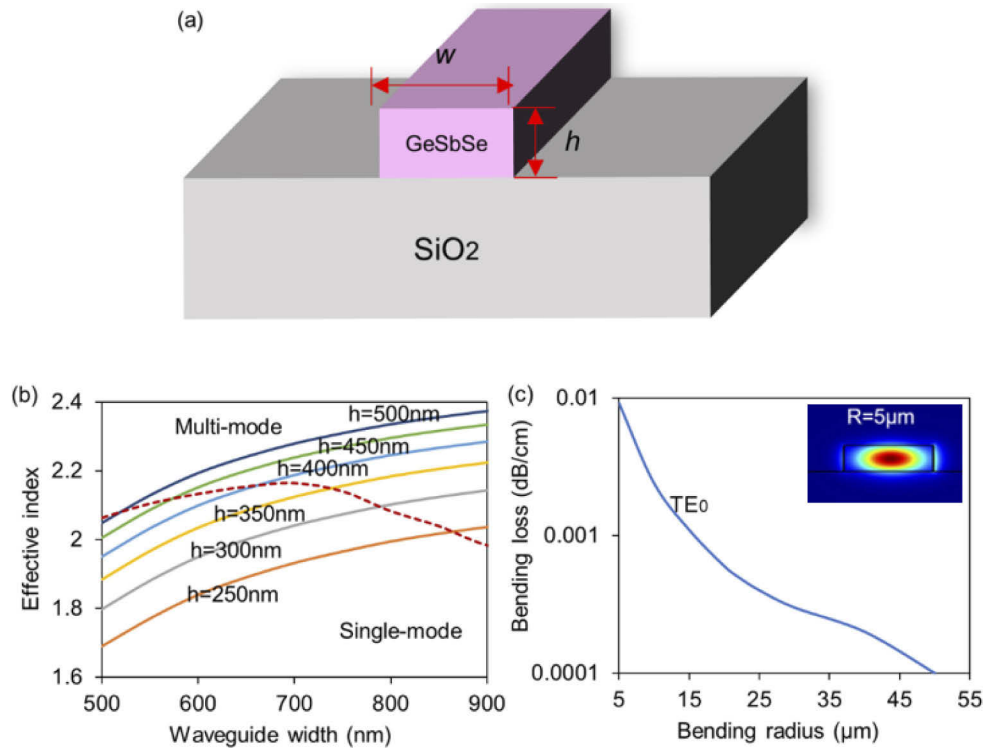
Fig. 1. (a) 3D cross-sectional view of the proposed GeSbSe photonic waveguide, (b) Calculated effective index of TE modes as a function of waveguide width for different heights. The red dashed curve indicates the boundary of single- and multi-mode operation, and (c) Calculated bending loss as a function of bending radius for TE_0 mode. Inset: the fundamental TE mode profile of a bending waveguide with a radius of 5 μm

characteristic. The zero-dispersion wavelength can be efficiently shifted over more than 200 nm (1500 to 1700 nm) when the width is increased by only 80 nm. Figure 2(b) shows the dispersion parameter at the waveguide width of 720 nm, indicating near-zero anomalous dispersion at 1550 nm that facilitates four-wave mixing and soliton-based nonlinear applications. The inset in Fig. 2(b) shows the simulated optical field of the fundamental TE mode of the 720 nm wide GeSbSe waveguide. Due to the strong mode confinement, the effective mode area (A_{eff}) is as small as 0.17 μm^2.

We calculate the waveguide nonlinear coefficient of the waveguide with the definition $\gamma = 2\pi n_2 / \lambda A_{\text{eff}}$ [1], where n_2 is the nonlinear refractive index [30]. Compared to the well-recognized low index-contrast waveguides, e.g., silicon nitride waveguide with typical A_{eff} of ~1.0 μm^2 and n_2 of 2.5×10^{-19} m^{2}W^{-1} [11,31], which is one orders of magnitude smaller than GeSbSe. The nonlinear coefficient γ of the proposed GeSbSe waveguide is calculated to be up to 110 W^{-1}m^{-1} at 1550 nm, which is more than 100 folds larger than that of silicon nitride waveguides. This nonlinear coefficient value is also comparable to that achieved in silicon nanowires [32].

We fabricated the photonic device in ChG using the following process [33]. First, bulk GeSbSe glass was prepared by the traditional melt-quenching method [34]. A 300 nm thick GeSbSe film was deposited by thermal evaporation onto a 4-inch silicon wafer with a 2 μm thick thermal oxide layer, followed by a 30 nm thick SiO$_2$ film deposited by magnetron sputtering onto the surface of the GeSbSe film to protect chalcogenide films from damage during development.
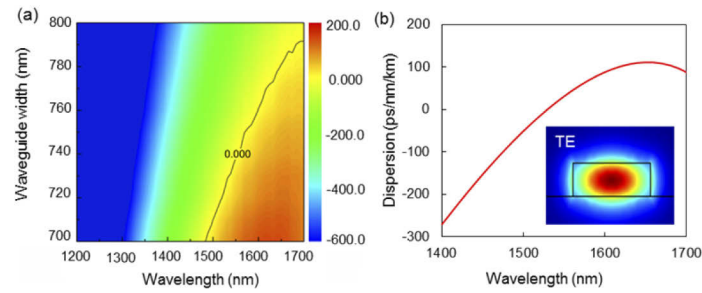
Fig. 2. (a) Calculated GVD (ps/nm/km) of the fundamental TE mode as a function of waveguide width and wavelength in 300 nm thickness GeSbSe waveguides. The black curve indicated the zero-dispersion wavelength. (b) The dispersion parameter of the waveguide with 720 nm width. The inset shows the simulated optical field of the fundamental TE mode

Then, the devices were patterned with a 200 nm thick ARP6200 photoresist using electron beam lithography (RAITH e-LINE Plus). The exposed structures underwent a plasma treatment step with O_2/Ar/CHF_3 gases to remove residues after the development process. Subsequently, the underlying GeSbSe layer was fully etched utilizing a mixture gas of CHF_3 and CF_4 at low pressure via inductively coupled plasma (ICP) etching (Oxford 100). After etching, the resist residue was removed by oxygen plasma cleaning and then soaking the sample in N-methyl-2-pyrrolidone (NMP) for 5 min. Figure 3(a) shows a scanning electron microscope (SEM) image of the fabricated GeSbSe waveguide cross section. A vertical sidewall is achieved with a good anisotropy, showing the high quality of the fabrication procedures. Figure 3(b) shows a waveguide coupled $Ge_{28}Sb_{12}Se_{60}$ microring, and the coupling region marked by the red box is enlarged in Fig. 3(c), where a clear interface feature indicates a good pattern definition in our process.
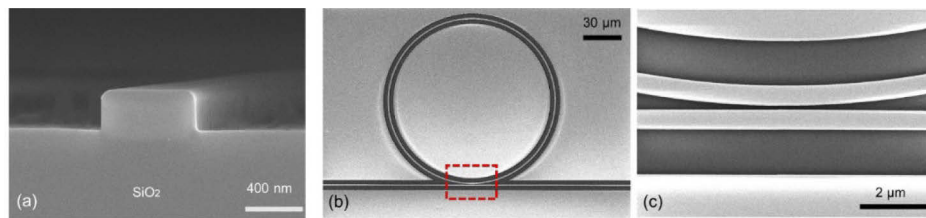

Fig. 3. Cross-section SEM image of a fabricated GeSbSe waveguide. (b) SEM image of a GeSbSe microring coupled with a bus waveguide. (c) Close-up of the coupling region as denoted by the dashed box in (b)

3. Device characterization

Fully etched fiber-waveguide grating couplers were fabricated to measure the microring resonators. In the experiments, continuous wave with sub-MHz linewidth from the tunable laser (Santac TSL-550) was coupled into and out of the waveguides by first-order Bragg scatting via grating couplers collected on the other side of the waveguides into a low-noise power meter (Santec MPM210) via single-mode fibers. The power of the coupled light was selected to be low enough (~ 0.1 mW) to minimize any nonlinear effects. We measured the spectral response of the regular fully etched grating couplers (not shown here). The spectra suffer from severe oscillation ripples with an extinction ratio of ~5 dB due to the high index contrast of GeSbSe gratings. A sub-wavelength grating coupler was introduced to dramatically reduce the Fresnel reflection coefficient to alleviate this issue [35]. Figure 4(a) shows a scanning electron microscopy

(SEM) image of the proposed sub-wavelength grating coupler. The optimized sub-wavelength grating coupler for the TE mode has 920 nm grating period, 538 nm grating width, and 83 nm sub-wavelength grating width. The incident angle for the sub-wavelength TE grating couplers is 10°. Figure 4(b) shows the measured spectral response of a fully etched sub-wavelength grating coupler with slight ripples. The peak coupling efficiency for a single grating is measured to be ~21% (-6.8 dB) from the experimental data.
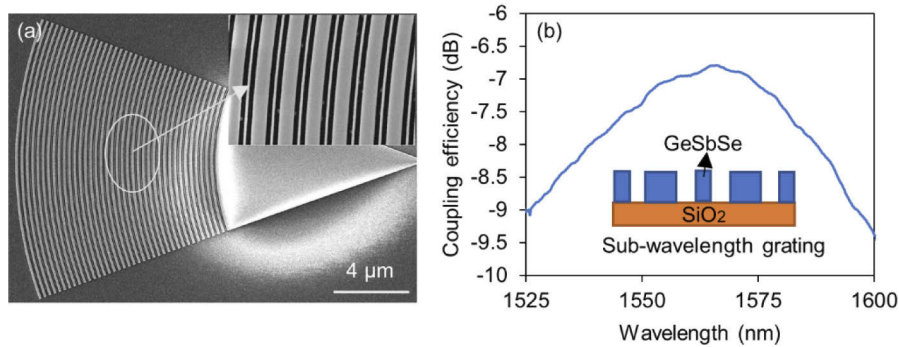

Fig. 4. (a) The SEM image of the fabricated focusing sub-wavelength grating coupler. (b) Grating coupler efficiency versus wavelength.

We analyzed a series of ring resonators with a radius of 90 μm (see Fig. 2(b)) to characterize the optical quality factor at telecom wavelengths. To study the coupling behavior of the resonators, we fabricated identical devices with coupling gaps varying from 100 nm to 300 nm, thus allowing us to examine ring resonators in both the over-coupled and under-coupled regimes [36]. The gap between the ring resonator and waveguide is 180 nm when reaching the critical coupling condition. Figure 5(a) shows a representative transmission spectrum of the resonators for TE_0 mode. Only one mode family with a free spectral range (FSR) of ~1.35 nm was observed in the spectrum, implying that the resonator with anomalous dispersion can be a single-mode operation. When the coupling gap was optimized for critical coupling, we found an extinction ratio up to 23 dB. Figure 5(b) shows the loaded Q-factor (Q_l) is estimated to be 2.1×10^5 by fitting the individual resonance with a full width at half maximum (FWHM) of 7.4 pm using the Lorentzian model. The intrinsic Q-factor (Q_i) of the resonator is calculated to be 4.1×10^5 by using the equation $Q_i = 2Q_{load}/(1 + \sqrt{T_0})$ for under-coupled devices [37], where Q_{load} is the measured loaded Q, and T_0 is the fraction of transmitted power at resonance wavelength. The propagation loss α (in cm^{-1}) was calculated by [38],
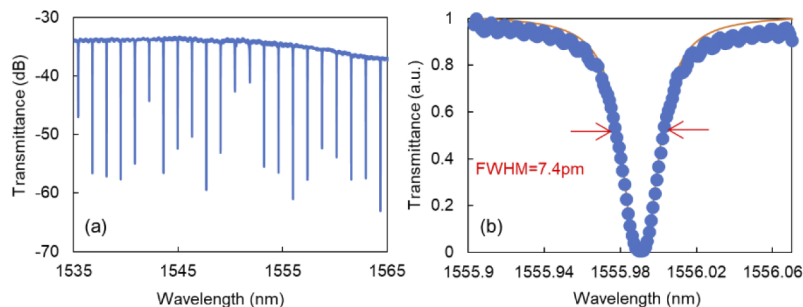

Fig. 5. (a) The spectrum for an under-coupled ring resonator. (b) The Lorentzian fit to the resonance dip (solid red line) reveals a linewidth of 7.4 pm corresponding to optical Q of 210,000.

$$\alpha = \frac{2\pi n_g}{Q_{in}\lambda_r} \tag{1}$$

where λ_r is the resonant wavelength, and Q_{in} represents the intrinsic quality factor. The group refractive index n_g is correlated with the free spectral range (FSR) via,

$$n_g = \frac{\lambda_r^2}{L \times FSR} \tag{2}$$

where L is the perimeter of the ring resonator. A small propagation loss of $\alpha = 1.3$ dB/cm is obtained using Eq. (1). The intrinsic Q_i of microring resonator is caused by several factors: intrinsic radiative losses (Q_{rad}^{-1}), material absorption losses (Q_m^{-1}), scattering loss due to surface inhomogeneities (Q_s^{-1}), i.e., the intrinsic Q_i can be expressed as:

$$Q_i^{-1} = Q_{rad}^{-1} + Q_{mat}^{-1} + Q_s^{-1} \tag{3}$$

Here Q_i is measured to be 4.1×10^5, Q_{rad} is calculated to be $\sim 5.2 \times 10^{17}$ using COMSOL Multiphysics when the radius is 90 um, Q_{mat} is estimated to be 2.9×10^6 through the formula $Q_{mat} = 2\pi n_g/\alpha\lambda$ [39], where n_g is the group index of material, α is the absorption loss of material [40]. Our measured Q_i factors are much smaller than both Q_{rad} and Q_{mat}, suggesting that the Q factor is limited by the scattering loss from the surface and edge of the waveguide. We can further enhance the Q factor for the GeSbSe microresonators by optimizing the fabrication process. Here the waveguide loss comes mainly from the sidewall roughness since it can be further reduced by increasing the waveguide width in our experiment. Recently, M. Grayson et al. reported that the GeSbSe waveguide loss could be decreased to 1 dB/cm by the thermal annealing process [41]. However, the cross-sectional geometry of the reflowed waveguide is severely deformed, which prevents them from efficient dispersion engineering on demand of emerging nonlinear applications. B. Zhang *et al.* have proposed a unique method to optimize the waveguide fabrication process using polymer-assisted thermal treatment, which shows a great potential to reduce the waveguide loss with an unchanged geometry [42]. Table 1 summarizes several submicron waveguides reported with different ChG materials. Here, we use the attenuation-related figure-of-merit (FOM) defined by γ/α [42]. As shown in Table 1, the FOM of the GeSbSe waveguide is the highest one among these platforms, which makes it the most suitable platform for nonlinear parametric processes. In addition, the linear refractive index of GeSbSe is larger than those of the other platforms, enabling compact circuits and efficient dispersion engineering. For the platforms based on GeSbSe, our device shows superior FOM, which is 4-folds higher than that in [43].

Table 1. Summary of linear and nonlinear characteristics of reported submicron chalcogenide waveguides at 1550 nm.

Materias	N	n_2 (m^{2}W^{-1})	Mode area (μm^2)	γ (W^{-1}m^{-1})	α (dB/cm)	FOM$_\alpha$ (γ/α) (W^{-1})	Reference
Ge$_{11.5}$As$_{24}$Se$_{64.5}$	2.66	8.6×10^{-18}	0.24	136	2.6	2.27	[23]
Ge$_{11.5}$As$_{24}$Se$_{64.5}$	2.7	7.6×10^{-18}	0.35	88.1	1.7	2.25	[44]
Ge$_{23}$Sb$_7$S$_{70}$	2.22	0.93×10^{-18a}	0.29	13.1	0.5	1.14	[38]
Ge$_{23}$Sb$_7$S$_{70}$	2.22	0.93×10^{-18a}	0.58	6.5	0.84	0.34	[45]
Ge$_{22}$Sb$_{18}$Se$_{60}$	2.73	5.1×10^{-18}	0.27	77.7	4	0.84	[43]
Ge$_{28}$Sb$_{12}$Se$_{60}$	2.8	5.12×10^{-18}	0.19	110	1.3	3.67	(This work)

[a]The nonlinear refractive index of Ge$_{23}$Sb$_7$S$_{70}$ is from [46].

4. Thermal characteristics on the ChG microring

We further characterized the thermo-optical properties of the GeSbSe microring resonator. In the experiment, a thermoelectric controller (TEC) was placed beneath the chip to accurately control the temperature of the substrate. Figure 6(a) shows the measured transmission spectrum of the ring resonators with temperatures range from 20°C to 60°C at a step of 5°C, which shows that the resonant wavelength increases with the temperature. Figure 6(b) shows that the wavelength drift induced by temperature is linear, indicating the temperature-dependent resonant wavelength shift $d\lambda_{res}/dT$ ~63.4 pm/K. The temperature-dependent resonance wavelength shift for a ring resonator is mainly attributed to both thermal-optical and thermal expansion effects, which is given by [47].
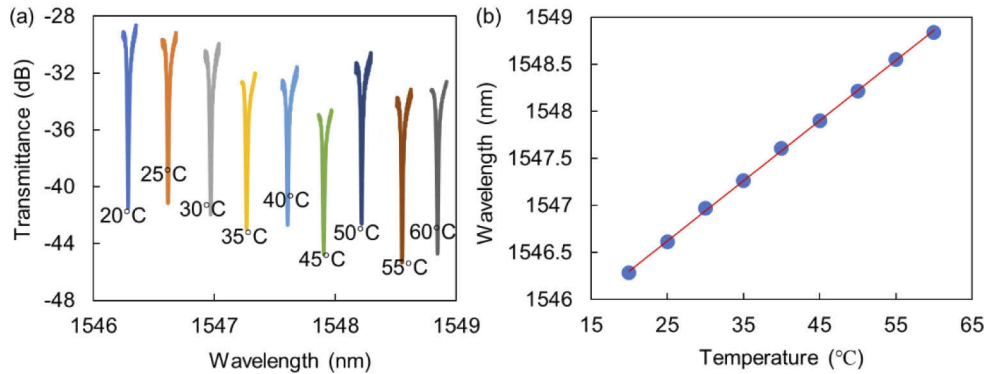

Fig. 6. (a) Transmission vs. wavelength for a resonant mode in the mirroring with a radius of 90 μm at different ambient temperatures. (b) Measured resonant wavelength (blue dots) as a function of temperature with linear fitting (red line).

$$\frac{d\lambda_{res}}{dT} = \lambda_{res}\left(\frac{1}{n_{eff}}\frac{dn_{eff}}{dT} + \frac{1}{R}\frac{dR}{dT}\right) \quad (4)$$

where λ_{res} is the resonant wavelength, n_{eff} is the effective index of resonant mode, and R is the principal radius of the microring. Since the optical mode is highly confined in the ChG waveguide core, the temperature-dependent effective index of optical mode is primarily determined by the thermo-optic coefficient of the material, indicating $(1/n_0)C_{TOC} \equiv (1/n_0)(dn_0/dT) = (1/n_{eff})(dn_{eff}/dT)$ with n_0 being the refractive index of bulk ChG. Using the linear thermal expansion coefficient $C_{CTE} \equiv 1/R \times dR/dT$ of 1.4×10^{-5}/K for GeSbSe glass at room temperature [33,40], the thermo-optic coefficient C_{TOC} can be approximated from Eq. (3) as 5.66×10^{-5}/K, which is in agreement with those reported in [40].

5. Conclusion

We have successfully fabricated dispersion-engineered chalcogenide microring resonators in high index-contrast GeSbSe ChG waveguide using e-beam lithography and plasma etching. A microring resonator with a radius of 90 μm shows an intrinsic Q around 4.1×10^5 at 1550 nm, which is comparable with the previously reported Qs of ChG microrings with different compositions [38,44,45]. Benefitting from the submicron mode confinement, the nonlinear coefficient is up to $110W^{-1}$ m^{-1}, which is one of the highest achievable values among ChG waveguide platforms. In addition, a single grating coupler with high peak efficiency of 21% was achieved. The thermal responses for the resonant wavelength of the microring were measured to be ~63.4 pm/K, and the thermo-optic coefficient of GeSbSe was extracted to be 5.66 ×

10^{-4}/K. Hence, ChG microring resonators with advantages of dispersion engineering, high-*Q*, and high-nonlinearity can find rich applications in power-efficient nonlinear photonics.

References

1. J. Leuthold, C. Koos, and W. Freude, "Nonlinear silicon photonics," Nat. Photonics **4**(8), 535–544 (2010).
2. P. Marin-Palomo, J. N. Kemal, M. Karpov, A. Kordts, J. Pfeifle, M. H. P. Pfeiffer, P. Trocha, S. Wolf, V. Brasch, M. H. Anderson, R. Rosenberger, K. Vijayan, W. Freude, T. J. Kippenberg, and C. Koos, "Microresonator-based solitons for massively parallel coherent optical communications," Nature, **546** (7657), 274–279 (2017).
3. M. Kues, C. Reimer, J. M. Lukens, W. J. Munro, A. M. Weiner, D. J. Moss, and R. Morandotti, "Quantum optical microcombs," Nat. Photonics **13**(3), 170–179 (2019).
4. D. Grassani, E. Tagkoudi, H. Guo, C. Herkommer, F. Yang, T. J. Kippenberg, and C.-S. Brès, "Mid infrared gas spectroscopy using efficient fiber laser driven photonic chip-based supercontinuum," Nat. Commun. **10**(1), 1553 (2019).
5. A. L. Gaeta, M. Lipson, and T. J. Kippenberg, "Photonic-chip-based frequency combs," Nat. Photonics **13**(3), 158–169 (2019).
6. J. Yuan, Z. Kang, F. Li, X. Zhang, X. Sang, Q. Wu, B. Yan, K. Wang, X. Zhou, K. Zhong, G. Zhou, C. Yu, C. Lu, H. Y. Tam, and P. K. A. Wai, "Mid-Infrared Octave-Spanning Supercontinuum and Frequency Comb Generation in a Suspended Germanium-Membrane Ridge Waveguide," J. Lightwave Technol. **35**(14), 2994–3002 (2017).
7. W. Mathlouthi, H. Rong, and M. Paniccia, "Characterization of efficient wavelength conversion by four-wave mixing in sub-micron silicon waveguides," Opt. Express **16**(21), 16735–16745 (2008).
8. K. Dolgaleva, P. Sarrafi, P. Kultavewuti, K. M. Awan, N. Feher, J. S. Aitchison, L. Qian, M. Volatier, R. Arès, and V. Aimez, "Tuneable four-wave mixing in AlGaAs nanowires," Opt. Express **23**(17), 22477–22493 (2015).
9. M. Pu, H. Hu, L. Ottaviano, E. Semenova, D. Vukovic, L. K. Oxenlowe, and K. Yvind, "Ultra-Efficient and Broadband Nonlinear AlGaAs-on-Insulator Chip for Low-Power Optical Signal Processing," Laser & Photonics Review **12**(12), 1800111 (2018).
10. K. J. A. Ooi, D. K. T. Ng, T. Wang, A. K. L. Chee, S. K. Ng, Q. Wang, L. K. Ang, A. M. Agarwal, L. C. Kimerling, and D. T. H. Tan, "Pushing the limits of CMOS optical parametric amplifiers with USRN:Si$_7$N$_3$ above the two-photon absorption edge," Nat. Commun. **8**(1), 13878 (2017).
11. J. S. Levy, A. Gondarenko, M. A. Foster, A. C. Turner-Foster, A. L. Gaeta, and M. Lipson, "CMOS-compatible multiple-wavelength oscillator for on-chip optical interconnects," Nat. Photonics **4**(1), 37–40 (2010).
12. A. C. Turner, M. A. Foster, A. L. Gaeta, and M. Lipson, "Ultra-low power parametric frequency conversion in a silicon microring resonator," Opt. Express **16**(7), 4881–4887 (2008).
13. A. D. Bristow and N. v. H. M. Rotenberg, Driel, "Two-photon absorption and Kerr coefficients of silicon for 850–2200 nm," Appl. Phys. Lett. **90**(19), 191104 (2007).
14. B. J. Eggleton, B. Lutherdavies, and K. Richardson, "Chalcogenide photonics," Nat. Photonics **5**(3), 141–148 (2011).
15. H. Shang, D. Sun, M. Zhang, J. Song, Z. Yang, D. Liu, S. Zeng, L. Wan, B. Zhang, Z. Wang, Z. Li, and Y.-G. Liu, "On-Chip Detector Based on Supercontinuum Generation in Chalcogenide Waveguide," J. Lightwave Technol. **39**(12), 3890–3895 (2021).
16. J. S. Sanghera, C. M. Florea, L. B. Shaw, P. Pureza, V. Q. Nguyen, M. Bashkansky, Z. Dutton, and I. D. Aggarwal, "Non-linear properties of chalcogenide glasses and fibers," J. Non-Cryst. Solids **354**(2-9), 462–467 (2008).
17. T. Wang, X. Gai, W. Wei, R. Wang, Z. Yang, X. Shen, S. Madden, and B. Luther-Davies, "Systematic z-scan measurements of the third order nonlinearity of chalcogenide glasses," Opt. Mater. Express **4**(5), 1011–1022 (2014).
18. A. Prasad, C. J. Zha, R. P. Wang, A. Smith, and B. Luther-Davies, "Properties of GexAsySe1-x-y glasses for all-optical signal processing," Opt. Express **16**(4), 2804–2815 (2008).
19. H. Lin, Y. Song, Y. Huang, D. Kita, S. Deckoff-Jones, K. Wang, L. Li, J. Li, H. Zheng, Z. Luo, H. Wang, S. Novak, A. Yadav, C.-C. Huang, R.-J. Shiue, D. Englund, T. Gu, D. Hewak, K. Richardson, J. Kong, and J. Hu, "Chalcogenide glass-on-graphene photonics," Nat. Photonics **11**(12), 798–805 (2017).
20. P. Ma, D.-Y. Choi, Y. Yu, Z. Yang, K. Vu, T. Nguyen, A. Mitchell, B. Luther-Davies, and S. Madden, "High Q factor chalcogenide ring resonators for cavity-enhanced MIR spectroscopic sensing," Opt. Express **23**(15), 19969–19979 (2015).
21. Z. Han, P. Lin, V. Singh, L. Kimerling, J. Hu, K. Richardson, A. Agarwal, and D. T. H. Tan, "On-chip mid-infrared gas detection using chalcogenide glass waveguide," Appl. Phys. Lett. **108**(14), 141106 (2016).

22. Y. Yu, X. Gai, P. Ma, K. Vu, Z. Yang, R. Wang, D.-Y. Choi, S. Madden, and B. Luther-Davies, "Experimental demonstration of linearly polarized 2–10 μm supercontinuum generation in a chalcogenide rib waveguide," Opt. Lett. **41**(5), 958–961 (2016).

23. X. Gai, S. Madden, D.-Y. Choi, D. Bulla, and B. Luther-Davies, "Dispersion engineered $Ge_{11.5}As_{24}Se_{64.5}$ nanowires with a nonlinear parameter of $136W^{-1}m^{-1}$ at 1550 nm," Opt. Express **18**(18), 18866–18874 (2010).

24. D.-G. Kim, S. Han, J. Hwang, I. H. Do, D. Jeong, J.-H. Lim, Y.-H. Lee, M. Choi, Y.-H. Lee, D.-Y. Choi, and H. Lee, "Universal light-guiding geometry for on-chip resonators having extremely high Q-factor," Nat. Commun. **11**(1), 5933 (2020).

25. B. J. Eggleton, C. G. Poulton, and R. Pant, "Inducing and harnessing stimulated Brillouin scattering in photonic integrated circuits," Adv. Opt. Photonics **5**(4), 536–587 (2013).

26. B. Morrison, A. Casas-Bedoya, G. Ren, K. Vu, Y. Liu, A. Zarifi, T. G. Nguyen, D.-Y. Choi, D. Marpaung, S. J. Madden, A. Mitchell, and B. J. Eggleton, "Compact Brillouin devices through hybrid integration on silicon," Optica **4**(8), 847–854 (2017).

27. Z. Li, Q. Du, C. Wang, J. Zou, T. Du, K. A. Richardson, Z. Cai, J. Hu, and Z. Luo, "Externally Pumped Photonic Chip-Based Ultrafast Raman Soliton Source," Laser Photonics Rev. **15**(2), 2000301 (2021).

28. Y. Zhu, L. Wan, Z. Chen, Z. Yang, D. Xia, P. Zeng, J. Song, J. Pan, Y. Feng, M. Zhang, W. Liu, J. Li, B. Zhang, and Z. Li, "Effects of Shallow Suspension in Low-Loss Waveguide-Integrated Chalcogenide Microdisk Resonators," J. Lightwave Technol. **38**(17), 4817–4823 (2020).

29. S. J. Madden, D. Y. Choi, D. A. Bulla, A. V. Rode, B. Luther-Davies, V. G. Ta'eed, M. D. Pelusi, and B. J. Eggleton, "Long, low loss etched As_2S_3 chalcogenide waveguides for all-optical signal regeneration," Opt. Express **15**(22), 14414–14421 (2007).

30. J. Zhou, Q. Du, P. Xu, Y. Zhao, R. Lin, Y. Wu, P. Zhang, W. Zhang, and X. Shen, "Large Nonlinearity and Low Loss Ge-Sb-Se Glass Photonic Devices in Near-Infrared," IEEE J. Sel. Top. Quantum Electron. **24**(4), 1–6 (2018).

31. M. Pu, L. Ottaviano, E. Semenova, and K. Yvind, "Efficient frequency comb generation in AlGaAs-on-insulator," Optica **3**(8), 823–826 (2016).

32. M. A. Foster, A. C. Turner, M. Lipson, and A. L. Gaeta, "Nonlinear optics in photonic nanowires," Opt. Express **16**(2), 1300–1320 (2008).

33. R. Zhang, Z. Yang, M. Zhao, P. Xu, W. Zhang, Z. Kang, J. Zheng, S. Dai, R. Wang, and A. Majumdar, "High quality, high index-contrast chalcogenide microdisk resonators," Opt. Express **29**(12), 17775–17783 (2021).

34. W.-H. Wei, R.-P. Wang, X. Shen, L. Fang, and B. Luther-Davies, "Correlation between Structural and Physical Properties in Ge–Sb–Se Glasses," J. Phys. Chem. C **117**(32), 16571–16576 (2013).

35. Y. Wang, X. Wang, J. Flueckiger, H. Yun, W. Shi, R. Bojko, N. A. F. Jaeger, and L. Chrostowski, "Focusing sub-wavelength grating couplers with low back reflections for rapid prototyping of silicon photonic circuits," Opt. Express **22**(17), 20652–20662 (2014).

36. W. Bogaerts, P. De Heyn, T. Van Vaerenbergh, K. De Vos, S. Kumar Selvaraja, T. Claes, P. Dumon, P. Bienstman, D. Van Thourhout, and R. Baets, "Silicon microring resonators," Laser & Photonics Reviews **6**(1), 47–73 (2012).

37. P. E. Barclay, K. Srinivasan, and O. Painter, "Nonlinear response of silicon photonic crystal microresonators excited via an integrated waveguide and fiber taper," Opt. Express **13**(3), 801–820 (2005).

38. Q. Du, Y. Huang, J. Li, D. Kita, J. Michon, H. Lin, L. Li, S. Novak, K. Richardson, W. Zhang, and J. Hu, "Low-loss photonic device in Ge–Sb–S chalcogenide glass," Opt. Lett. **41**(13), 3090–3093 (2016).

39. M. L. Gorodetsky, A. A. Savchenkov, and V. S. Ilchenko, "Ultimate Q of optical microsphere resonators," Opt. Lett. **21**(7), 453–455 (1996).

40. Schott Infrared Chalcogenide Glasses Datasheet, http://www.schott.com/d/advanced_optics/a8acc8e2-8855-4be6-8b2a-e4b2ada72a15/1.0/schott-infrared-chalcog-glasses-irg25-january-2016-eng.pdf.

41. M. Grayson, M. Zohrabi, K. Bae, J. Zhu, J. T. Gopinath, and W. Park, "Enhancement of third-order nonlinearity of thermally evaporated GeSbSe waveguides through annealing," Opt. Express **27**(23), 33606–33620 (2019).

42. B. Zhang, P. Zeng, Z. Yang, D. Xia, Y. Sun, Y. Huang, J. Song, J. Pan, H. Cheng, D. Y. Choi, and Z. Li, "On-chip Chalcogenide Microresonators with Low Threshold Parametric Oscillation," Photonics Res. **9**(7), 1272–1279 (2021).

43. Q. Du, Z. Luo, H. Zhong, Y. Zhang, Y. Huang, T. Du, W. Zhang, T. Gu, and J. Hu, "Chip-scale broadband spectroscopic chemical sensing using an integrated supercontinuum source in a chalcogenide glass waveguide," Photonics Res. **6**(6), 506–510 (2018).

44. W. C. Jiang, K. Li, X. Gai, D. A. Nolan, and P. Dainese, "Ultra-low-power four-wave mixing wavelength conversion in high-Q chalcogenide microring resonators," Opt. Lett. **46**(12), 2912–2915 (2021).

45. J. Chiles, M. Malinowski, A. Rao, S. Novak, K. Richardson, and S. Fathpour, "Low-loss, submicron chalcogenide integrated photonics with chlorine plasma etching," Appl. Phys. Lett. **106**(11), 111110 (2015).

46. S. Serna, H. Lin, C. Alonso-Ramos, A. Yadav, X. Le Roux, K. Richardson, E. Cassan, N. Dubreuil, J. Hu, and L. Vivien, "Nonlinear optical properties of integrated GeSbS chalcogenide waveguides," Photonics Res. **6**(5), B37–B42 (2018).

47. Q. Zhao, R. O. Behunin, P. T. Rakich, N. Chauhan, A. Isichenko, J. Wang, C. Hoyt, C. Fertig, M.h Lin, and D. J. Blumenthal, "Low-loss low thermo-optic coefficient Ta_2O_5 on crystal quartz planar optical waveguides," APL Photonics **5**(11), 116103 (2020).